Computers & Fluids 67 (2012) 115–122

Contents lists available at SciVerse ScienceDirect

Computers & Fluids

journal homepage: www.elsevier.com/locate/compfluid

Multiple temperature kinetic model and its applications to micro-scale gas flows

Hongwei Liu [a,*], Kun Xu [b], Taishan Zhu [c], Wenjing Ye [c]

[a] State Key Laboratory of High Temperature Gas Dynamics, Institute of Mechanics, Chinese Academy of Sciences, Beijing 100190, China
[b] Department of Mathematics, The Hong Kong University of Science and Technology, Kowloon, Hong Kong
[c] Department of Mechanical Engineering, The Hong Kong University of Science and Technology, Kowloon, Hong Kong

ARTICLE INFO

Article history:
Received 16 February 2012
Received in revised form 16 May 2012
Accepted 7 July 2012
Available online 15 July 2012

Keywords:
Non-equilibrium flows
Kinetic models
Rarefied gas dynamics
Gas-kinetic schemes

ABSTRACT

This paper presents a gas-kinetic scheme to solve the multiple temperature kinetic model (MTKM), which was proposed in J. Comput. Math. 29(6) (2011) 639–660, for the study of non-equilibrium flows. The MTKM is a two-stage particle collision model possessing an intermediate quasi-equilibrium state with a symmetric second-order temperature tensor. A gas-kinetic finite volume scheme is developed for the numerical solution of the MTKM in the continuum and transition flow regimes. The gas-kinetic scheme is designed for the updating of macroscopic variables, which include the conservative flow variables and the multiple temperature field. In order to validate the kinetic model, the gas-kinetic scheme is used in the study of lid-driven cavity flows in both continuum and transition flow regimes. The numerical results predicted by the MTKM are compared with those from the direct simulation Monte Carlo (DSMC) method, the Navier–Stokes equations (NSE), and the early three-temperature kinetic model (TTKM) proposed in Phys. Fluids 19, 016101(2007). It is demonstrated that the MTKM has obvious advantages in comparison with the NSE and the TTKM in capturing the non-equilibrium flow behavior in the transition flow regime. One distinguishable phenomenon captured by the MTKM is that in the transition flow regime the heat flux direction can be from a low temperature to a high temperature region, which violates the Fourier's law of continuum flows. The MTKM provides a more accurate physical model than the NSE for the non-equilibrium flows.

1. Introduction

Gas flows can be categorized into different flow regimes based on the Knudsen number Kn. In the continuum regime ($Kn < 0.001$), the Navier–Stokes equations (NSE) are adequate to model the fluid behavior. In the near continuum regime ($0.001 < Kn < 1$), the NSE are known to lose accuracy or be inadequate. In fact this regime is encountered in many practical engineering problems, for example those in aerospace engineering and Micro-Electro-Mechanical Systems (MEMS). Therefore, how to realize reliable numerical simulations of gas flows in this regime at low computational costs are of great interest from both scientific and practical views.

Currently the direct simulation Monte Carlo (DSMC) method is one of the most successful techniques for the non-equilibrium gas flows. However, the DSMC becomes very inefficient for near continuum and low speed flows because of the cell size restriction and the statistical noise. Various modifications have been proposed in order to improve the efficiency of the standard DSMC, for example the information preservation (IP) method [3–6], the variance reduction approach [7], the low Mach number DSMC algorithm [8] and the hybrid methods [9,10], just to name a few. Alternative methods, which directly solve the Boltzmann or model equations [11–15], have also attracted increasing attentions recently.

One of the continuum-based approaches in modeling the non-equilibrium flows is to use the high order governing equations derived from the Bhatnagar–Gross–Krook (BGK) model by the Chapman-Enskog expansion, for instance the Burnett and super-Burnett equations. However, it has been well recognized that these equations have the stability problems and cannot be directly used in numerical simulations [16]. In recent years, some improvements have been proposed in order to cure these problems [17–19]. Another strategy for non-equilibrium flow simulations is deriving various governing equations by the moment closure technique, such as Grad's 13 moment equations [20], the regularized 13 (R13) and 26 (R26) moment equations [21,22], Levermore's 10 moment system [23], and many others.

Recently, a multiple temperature kinetic model (MTKM) was proposed [1] for continuum and near continuum flow simulations, which is a nature extension of an early kinetic model [2,24]. The main difference between the two kinetic models is that the former defines the translational temperature as a second-order symmetric tensor while the latter only uses three translational temperatures in the x-, y- and z-directions. This is the reason that the latter is

* Corresponding author. Tel.: +86 10 82544022; fax: +86 10 62561284.
E-mail address: hliu@imech.ac.cn (H. Liu).

0045-7930/$ - see front matter © 2012 Elsevier Ltd. All rights reserved.
http://dx.doi.org/10.1016/j.compfluid.2012.07.006

renamed the three-temperature kinetic model (TTKM) here. In fact, prior to these two models, the gas-kinetic schemes describing the non-equilibrium flows related to the molecular rotational and vibrational degrees of freedom have been introduced for the shock structure calculations [25,26], where three different temperatures, i.e. the translational, rotational and vibrational temperatures, are used for modeling the non-equilibrium effects.

In [1], the generalized macroscopic gas dynamic equations based on the MTKM have been derived and analyzed, some quasi-one-dimensional numerical tests have been shown to demonstrate the performance of the MTKM in the micro-scale flow simulations. In the present work, instead of solving the corresponding macroscopic equations, a gas-kinetic scheme will be developed for the MTKM directly, and some truly two-dimensional (2D) test cases for the micro-scale gas flows will be presented in order to evaluate the capability of the MTKM in modeling the non-equilibrium flows.

2. Multiple temperature kinetic model and the gas-kinetic scheme

In this section, we briefly review the essentials of the MTKM and propose a finite volume gas-kinetic scheme as well as the wall boundary condition to get the numerical solutions of the MTKM.

2.1. A brief review of the MTKM

The three-temperature kinetic model for continuum and near continuum flows was proposed in [2], where only three translational temperatures for monotonic gases are used in the construction of the model. Numerical tests [2,24] have demonstrated some success of the TTKM in describing the non-equilibrium gas flows. However, the defects of the early model are also obvious: the applications of the model in numerical simulations will depend on the choice of the coordinate system, since only three translational temperatures in the x-, y- and z-directions are considered. Theoretically from the extended definition of temperature it should be a second-order symmetric tensor, in that case the model's utility will be independent of the coordinate system used.

These problems were cured in [1], where the temperature is defined as a second-order symmetric tensor and used to construct an improved gas-kinetic model, i.e. MTKM, for non-equilibrium flow simulations. The two-stage MTKM can be written as [1]

$$\frac{\partial f}{\partial t}+\mathbf{u}\cdot\nabla f=\frac{g-f}{\tau}+Q, \tag{1}$$

where t is the time, $\mathbf{u}=(u,v,w)$ is the velocity of the gas particle, τ is the collision time representing the relaxation rate of the distribution function f due to the collisions, $Q=(f^{eq}-g)/\tau$, which is treated as a special source term different from the term $(g-f)/\tau$ in the model [1], therefore, although this model is identical to the BGK model mathematically, the physical significance of two models is different. In the MTKM, the whole relaxation process of the non-equilibrium distribution function f to the Maxwellian equilibrium state f^{eq} is separated into two sub-processes: (i) f relaxes to an intermediate state g between f and f^{eq}; (ii) the intermediate distribution g relaxes to the Maxwellian equilibrium state f^{eq}. Although other choices may be possible, in our study the intermediate state g is assumed to be a Gaussian distribution

$$g=\frac{\rho}{\sqrt{\det(2\pi R\mathbf{T})}}\exp\left[-\frac{1}{2}(\mathbf{u}-\mathbf{U})(R\mathbf{T})^{-1}(\mathbf{u}-\mathbf{U})^{\mathrm{T}}\right], \tag{2}$$

where ρ is the density, R is the gas constant, $\mathbf{U}=(U,V,W)$ is the macroscopic velocity of the gas, $\mathbf{T}$ is the symmetric second-order temperature tensor, and for monatomic gas it reads

$$\mathbf{T}=\begin{pmatrix}T_{xx} & T_{xy} & T_{xz}\\ T_{xy} & T_{yy} & T_{yz}\\ T_{xz} & T_{yz} & T_{zz}\end{pmatrix}.$$

By taking moments $\Psi=(1,u_i,u_iu_j/2)^{\mathrm{T}}$ of Eq. (1) and using the Chapman-Enskog or iterative expansion, the following generalized gas dynamic (GGD) equations based on the MTKM can be derived [1],

$$\partial_t\rho+\partial_k(\rho U_k)=0, \tag{3}$$

$$\partial_t(\rho U_i)+\partial_k[\rho(U_iU_k+RT_{ik})]=\partial_k[\rho R(\overline{T}\delta_{ki}-T_{ki})], \tag{4}$$

$$\begin{aligned}&\partial_t[\rho(U_iU_j+RT_{ij})]+\partial_k[\rho(U_iU_jU_k+RU_kT_{ij}+RU_iT_{jk}+RU_jT_{ki})]\\&=\frac{2}{\tau}\rho R(\overline{T}\delta_{ij}-T_{ij})+\partial_k\{\rho R[U_k(\overline{T}\delta_{ij}-T_{ij})+U_i(\overline{T}\delta_{jk}-T_{jk})\\&\quad+U_j(\overline{T}\delta_{ki}-T_{ki})]\}-\partial_kQ_{ijk},\end{aligned} \tag{5}$$

where δ_{ij} is the Kronecker delta function, the averaged temperature $\overline{T}$ is obtained by

$$\overline{T}=\frac{1}{3}\sum_{l=1}^{3}T_{ll}, \tag{6}$$

and $\mathbf{Q}$ is the generalized heat flux given by

$$Q_{ijk}=-\frac{\tau\rho R^2}{\mathrm{Pr}}(T_{kl}\partial_lT_{ij}+T_{il}\partial_lT_{jk}+T_{jl}\partial_lT_{ki}), \tag{7}$$

where Pr is the Prandtl number.

Moreover, it has been shown by theoretical analysis in [1] that the standard NSE can be recovered from the first-order GGD equations in the continuum limit ($Kn\to 0$), which will also be clearly demonstrated by our numerical examples in this paper. Interested readers may refer to [1] for the construction of the MTKM, the detailed derivation and analysis of the GGD equations based on the MTKM for non-equilibrium gas flow simulations. One point that needs to be emphasized is that the numerical method presented in the next subsection is for the MTKM directly and the GGD equations are not explicitly used in the construction of the gas-kinetic scheme.

2.2. A numerical approach to solve the MTKM

Now we present the numerical approach to solve the MTKM. The numerical method for the MTKM is a finite volume scheme, which is similar to the numerical algorithm employed in [2] for the early TTKM. Both of the two methods are extensions from the gas-kinetic BGK solver for the NSE [31]. For simplicity, the 2D cases will be considered hereafter in this paper, but the scheme presented here can be also extended to three-dimensional problems.

For 2D gas flows, we have $T_{xz},T_{yz}=0$ for the temperature tensor $\mathbf{T}$. By taking moments, the macroscopic variables are defined as

$$\mathbf{W}=\int g\Psi_{2D}dudvdw=(\rho,\rho U,\rho V,E_{xx},E_{yy},E_{zz},E_{xy})^{\mathrm{T}}, \tag{8}$$

where

$$\Psi_{2D}=(1,u,v,u^2/2,v^2/2,w^2/2,uv/2)^{\mathrm{T}}, \tag{9}$$

and

$$E_{ij}=\rho(U_iU_j+RT_{ij})/2, \tag{10}$$

with $i,j=1,2,3$ representing x,y,z, respectively. Under the finite volume framework, for a uniform grid the updating of the cell-averaged value $\mathbf{W}_{p,q}$ over the cell (p,q) from the time t^n to t^{n+1} can be obtained by

$$\mathbf{W}_{p,q}^{n+1}=\mathbf{W}_{p,q}^{n}+\frac{1}{\Delta x}\left(F^{x,\Delta t}_{p-\frac{1}{2},q}-F^{x,\Delta t}_{p+\frac{1}{2},q}\right)+\frac{1}{\Delta y}\left(F^{y,\Delta t}_{p,q-\frac{1}{2}}-F^{y,\Delta t}_{p,q+\frac{1}{2}}\right)+\mathbf{S}^{\Delta t}_{p,q}, \tag{11}$$

where $F^{x,\Delta t}$ and $F^{y,\Delta t}$ are numerical fluxes during the time interval Δt $(= t^{n+1} - t^n)$ in x and y directions, respectively. The source term $\mathbf{S}$ is written as

$$\mathbf{S} = \left(0, 0, 0, \alpha(\overline{T} - T_{xx}), \alpha(\overline{T} - T_{yy}), \alpha(\overline{T} - T_{zz}), -\alpha T_{xy}\right)^{\mathrm{T}}, \tag{12}$$

where $\alpha = \rho R/(2\tau)$. The relation among the dynamic viscosity coefficient μ, the averaged temperature $\overline{T}$, and the relaxation time τ is given by $\mu = \tau \rho R \overline{T}$.

From Eq. (11), the finite volume method for solving the MTKM can be divided into two parts: (i) the source term discretization; (ii) the calculation of numerical fluxes across cell interfaces. For the source term, we simply use the following first-order approximation

$$\mathbf{S}^{\Delta t}_{p,q} = \Delta t \mathbf{S}^{n}_{p,q}. \tag{13}$$

In calculating the numerical flux, instead of using the macroscopic GGD equations, we evaluate it from the distribution function f at the cell interface based on the MTKM. More specifically, we use the Chapman-Enskog expansion

$$f = g - \tau\left(\frac{\partial g}{\partial t} + u\frac{\partial g}{\partial x} + v\frac{\partial g}{\partial y}\right) + t\frac{\partial g}{\partial t} \tag{14}$$

to construct the distribution function at the cell interface, therefore we need to evaluate $\frac{\partial g}{\partial x}, \frac{\partial g}{\partial y}$ and $\frac{\partial g}{\partial t}$ first before using Eq. (14).

We can determine $\frac{\partial g}{\partial x}$ and $\frac{\partial g}{\partial y}$ from the spacial derivatives of the macroscopic variables $\frac{\partial \mathbf{W}}{\partial x}$ and $\frac{\partial \mathbf{W}}{\partial y}$ at the cell interface, respectively. Next we will show how to get $\frac{\partial g}{\partial x}$ from $\frac{\partial \mathbf{W}}{\partial x}$. First, we assume

$$\frac{\partial g}{\partial x} = g(\Psi_{2D})^{\mathrm{T}}\mathbf{a}, \tag{15}$$

where $(\Psi_{2D})^{\mathrm{T}}$ is the transpose of Ψ_{2D} and the unknown vector $\mathbf{a}$ is defined as

$$\mathbf{a} = (a_1, a_2, a_3, a_4, a_5, a_6, a_7)^{\mathrm{T}}. \tag{16}$$

Then, the unknown vector $\mathbf{a}$ can be acquired using the numerical techniques, such as the Gauss elimination method, to solve the following system of 7 equations with 7 unknowns $a_1 - a_7$,

$$\int \frac{\partial g}{\partial x}\Psi_{2D}\,du\,dv\,dw = \left(\int g\Psi_{2D}(\Psi_{2D})^{\mathrm{T}}\,du\,dv\,dw\right)\mathbf{a} = \mathbf{M}\mathbf{a} = \frac{\partial \mathbf{W}}{\partial x}, \tag{17}$$

where $\mathbf{M}$ is the matrix defined as

$$\mathbf{M} = \int g\Psi_{2D}(\Psi_{2D})^{\mathrm{T}}\,du\,dv\,dw. \tag{18}$$

We want to point out that unlike the gas-kinetic schemes for the NSE and TTKM shown in [2,31], where the determinations of $\mathbf{a}$ from $\frac{\partial \mathbf{W}}{\partial x}$ can be done in an analytic way, see the Appendix B in [31] for the NSE and the explicit formulations to get a_1 to a_6 shown in [2] for the TTKM, however, here it is almost impossible or at least very difficult to get the similar explicit formulations of $\mathbf{a}$ from $\frac{\partial \mathbf{W}}{\partial x}$ based on Eq. (17), therefore we have to use the numerical methods like the Gauss elimination algorithm to solve Eq. (17) numerically in order to get $\mathbf{a}$.

Once $\mathbf{a}$ is provided, we can get $\frac{\partial g}{\partial x}$ from Eq. (15). By a similar procedure, $\frac{\partial g}{\partial y}$ can be also obtained from $\frac{\partial \mathbf{W}}{\partial y}$ numerically. After determining $\frac{\partial g}{\partial x}$ and $\frac{\partial g}{\partial y}$, we may further assume

$$\frac{\partial g}{\partial t} = g(\Psi_{2D})^{\mathrm{T}}\mathbf{A}, \tag{19}$$

with the unknown vector $\mathbf{A}$ defined as

$$\mathbf{A} = (A_1, A_2, A_3, A_4, A_5, A_6, A_7)^{\mathrm{T}}. \tag{20}$$

Then, we can use the following relation to determine the unknown vector $\mathbf{A}$

$$\int \left(\frac{\partial g}{\partial t} + u\frac{\partial g}{\partial x} + v\frac{\partial g}{\partial y}\right)du\,dv\,dw = 0. \tag{21}$$

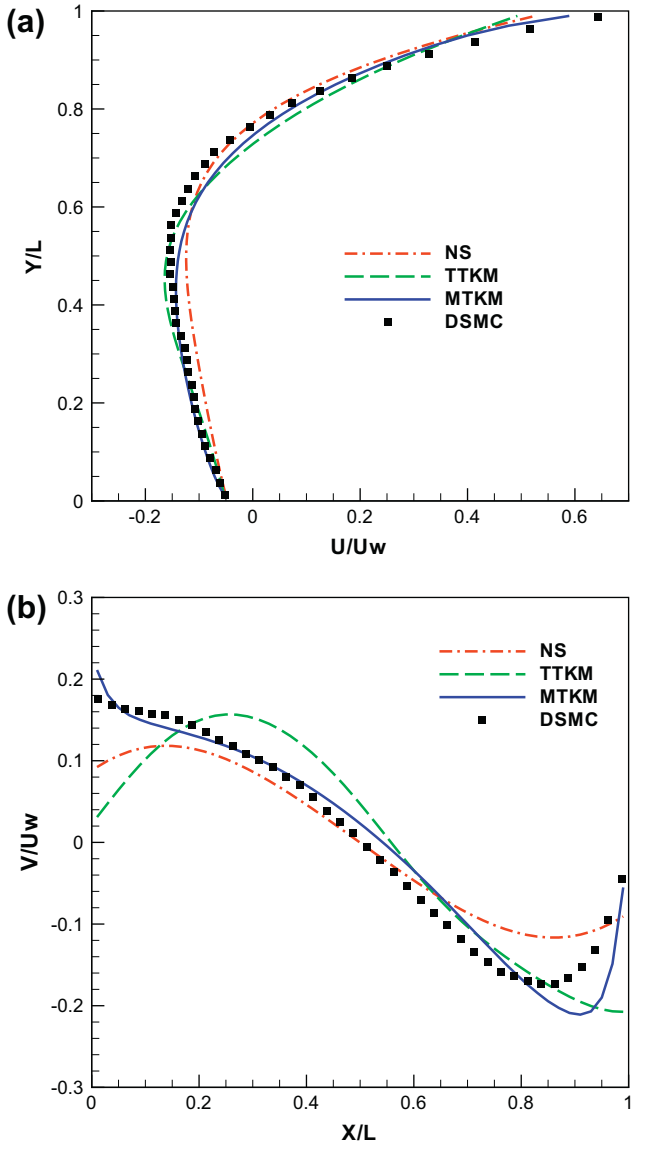

Fig. 1. Velocity profiles for the case with upper wall temperature 273 K and all other wall temperature 546 K, $U_w = 15.39$ m/s ($Ma = 0.05$) and $Kn = 0.1$. (a): The U-velocity along a vertical line crossing the cavity center; (b): The V-velocity along a horizontal line crossing the cavity center.

From Eqs. (19) and (21), we can get

$$\int \frac{\partial g}{\partial t}\Psi_{2D}\,du\,dv\,dw = \mathbf{M}\mathbf{A} = -\int \left(u\frac{\partial g}{\partial x} + v\frac{\partial g}{\partial y}\right)\Psi_{2D}\,du\,dv\,dw, \tag{22}$$

where $\mathbf{M}$ is defined by Eq. (18). Substituting $\frac{\partial g}{\partial x}$ and $\frac{\partial g}{\partial y}$ obtained earlier into Eq. (22), we reach a system of 7 equations with 7 unknowns $A_1 - A_7$, which is very similar to Eq. (17). Solving this system numerically, we can get $\mathbf{A}$, therefore $\frac{\partial g}{\partial t}$ is gained from Eq. (19).

Up to now we have obtained $\frac{\partial g}{\partial x}$, $\frac{\partial g}{\partial y}$ and $\frac{\partial g}{\partial t}$, so the time-dependent distribution function f at the cell interface can be totally determined from Eq. (14), which can be used to get the numerical flux in Eq. (11) by taking moments and integrating it over the time interval Δt. A modification of the heat flux in energy transport similar to those in [2,31] is implemented in order to model the flow with any realistic Prandtl number. The mathematical formulae for various moments of the Gaussian distribution g can be obtained by the software Mathematica.

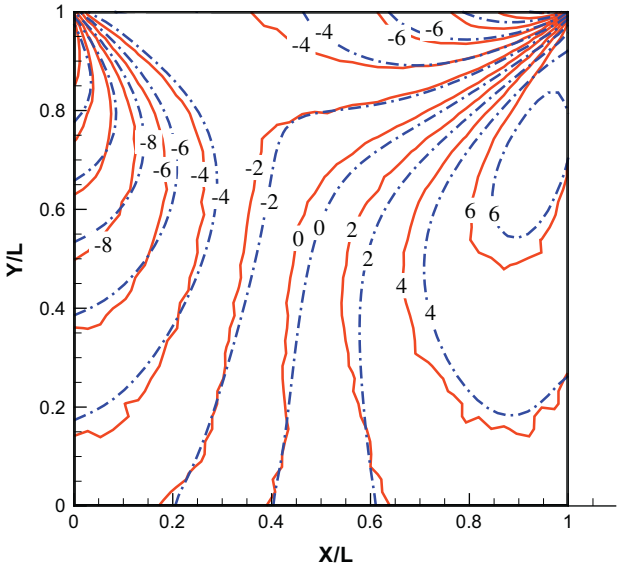

Fig. 2. The contours of T_{xy} predicted by DSMC (solid line) and MTKM (dash dot line) for the case with upper wall temperature 273 K and all other wall temperature 546 K, $U_w = 15.39$ m/s ($Ma = 0.05$) and $Kn = 0.1$.

2.3. Wall boundary condition

It is well known that the wall boundary condition is very important for the numerical simulations of the flows in the transition regime. In this paper, we use the strategy proposed in [32] to deal with the wall boundary condition for the MTKM. More specifically, with the one-sided interpolation of the macroscopic variables up to the wall, we can use the flow field information from the inner domain to evaluate the gas distribution function f^{in} at the inner side of the wall, for example Eq. (14) for the MTKM. Therefore, we can evaluate the number of particles hitting the wall from the inner side. In the following we will illustrate the boundary treatment by considering a stationary left vertical wall. For such a wall, the particle number hitting it during the time interval Δt from the inner side is $-\int_0^{\Delta t}\int_{u<0} uf^{in}dud\upsilon dwdt$. For the diffuse reflection part, we can construct an equilibrium state g^{out} at the outer side of the wall, i.e.

$$g^{out} = \rho_*\left(\frac{\lambda_*}{\pi}\right)^{\frac{3}{2}} e^{-\lambda_*(u^2+\upsilon^2+w^2)}, \tag{23}$$

where λ_* can be obtained from the given wall temperature T_w by the relation $\lambda_* = m/2kT_w$, m is the molecular mass and k is the Boltzmann constant. The density ρ_* in Eq. (23) can be determined from the requirement that no particles penetrate the wall, i.e.

$$\int_0^{\Delta t}\int_{u>0} ug^{out}dud\upsilon dwdt = -\int_0^{\Delta t}\int_{u<0} uf^{in}dud\upsilon dwdt, \tag{24}$$

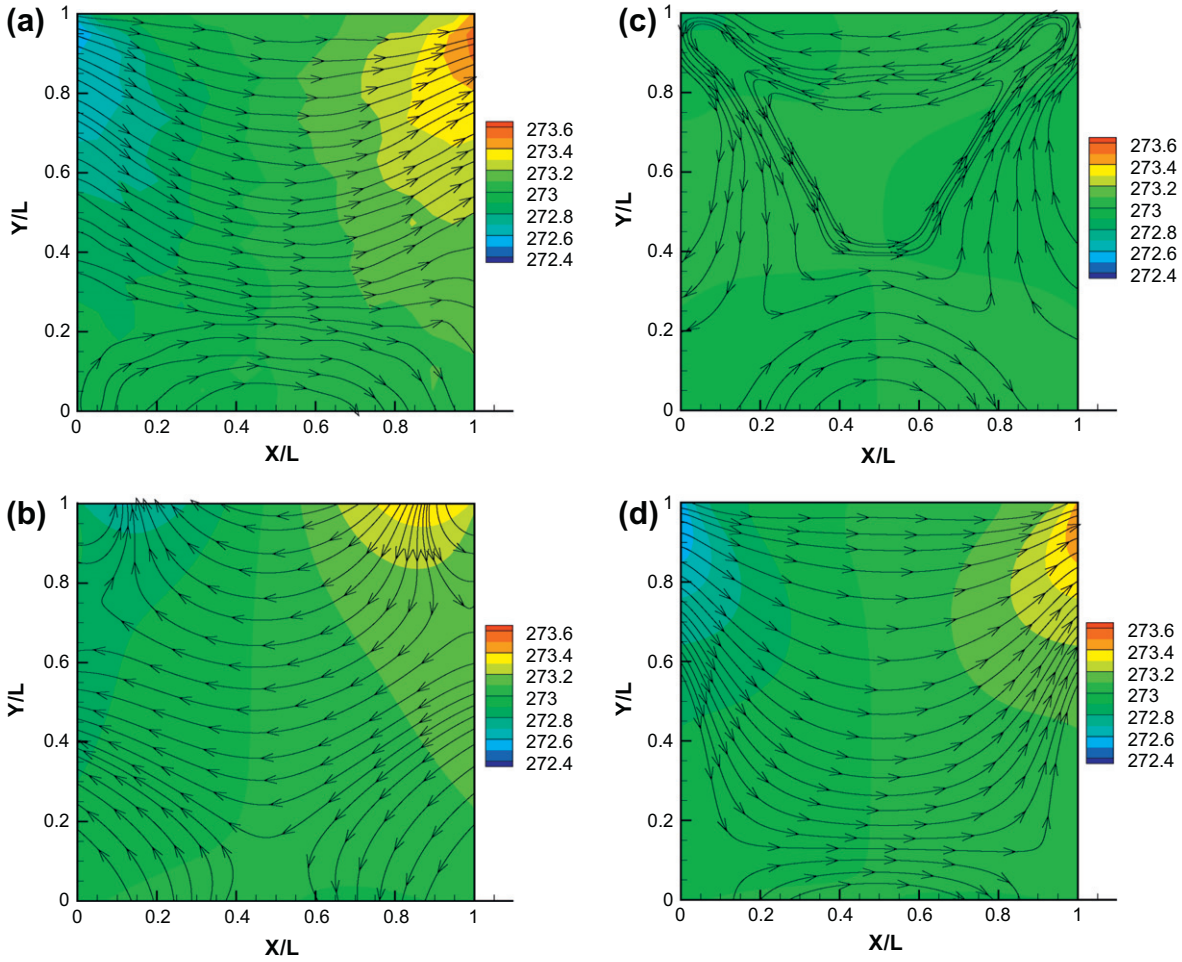

Fig. 3. Heat flux stream traces overlaid on the temperature $\overline{T}$ ($\overline{T} = (T_{xx} + T_{yy} + T_{zz})/3$) contours by (a) DSMC, (b) NSE, (c) TTKM and (d) MTKM for the case with all wall temperature 273 K, $U_w = 10$ m/s and $Kn = 0.2$.

from which the density ρ_* in the equilibrium state g^{out} can be obtained

$$\rho_* = -\frac{2\sqrt{\pi\lambda_*}}{\Delta t}\int_0^{\Delta t}\int_{u<0} u f^{in} du\, dv dw dt. \tag{25}$$

Therefore, given the accommodation coefficient σ, the total gas distribution function at the wall can be written as

$$f^{total} = f^{in}_{u<0} + \sigma g^{out}_{u>0} + (1-\sigma) f^{in}_{u<0}(-u, v, w), \tag{26}$$

where the term $(1-\sigma)f^{in}_{u<0}(-u,v,w)$ accounts for the specular reflection part from the wall. Once the distribution function f^{total} at the wall is obtained, taking moments and integrating over time, we can evaluate the numerical flux there required by the finite volume scheme for the MTKM.

We want to point out that this strategy of slip boundary treatment, i.e. Eqs. (23)–(26), can be also used for the NSE [33], the TTKM [2] and even the Burnett equations [32], where only the gas distribution function f^{in} at the inner side of the wall needs to be constructed based on different models. For example, for the NSE calculation the distribution function f^{in} in Eqs. (24)–(26) should be constructed using the NSE numerical solutions of the neighboring cells inside the computational domain [33], we may denote it by f^{in}_{NSE} here. Similarly, for the TTKM simulation [33], we need to construct f^{in}_{TTKM} in using Eqs. (24)–(26). Interested readers may refer to the above-mentioned papers for more details.

3. Numerical tests for micro-scale gas flows

In order to evaluate the performance of the MTKM, in this section we numerically study the 2D lid-driven cavity flows, which have been investigated extensively [27–30]. The numerical results predicted by the MTKM will be compared with those by the DSMC, the NSE and the early TTKM. In order to have a fair comparison, in this paper we use the same strategy, i.e. Eqs. (23)–(26), to treat the slip boundary conditions for the NSE, TTKM and MTKM simulations, and no special treatment is needed for the four corner cells of the computational domain.

In the present tests, the working gas is argon with the molecular mass $m = 6.63\times10^{-26}$ kg, the fully diffuse reflection is assumed for all walls. For all the numerical tests the initial gas state is set to be $T_0 = 273$ K and $p_0 = 1$ atm $= 101,325$ Pa, the dynamic viscosity coefficient μ is obtained by

$$\mu = \mu_0\left(\frac{\overline{T}}{T_0}\right)^{\omega}, \tag{27}$$

with $\mu_0 = 2.117\times10^{-5}$ Pa s and $\omega = 0.81$. The mean free path l of the gas is defined by

$$l = \frac{4(7-2\omega)(5-2\omega)}{30\sqrt{\pi}}\times\frac{\mu}{\rho\sqrt{2R\overline{T}}}. \tag{28}$$

In our numerical studies, the Knudsen number Kn is defined as the ratio of the mean free path l_0 at the initial gas state and the side

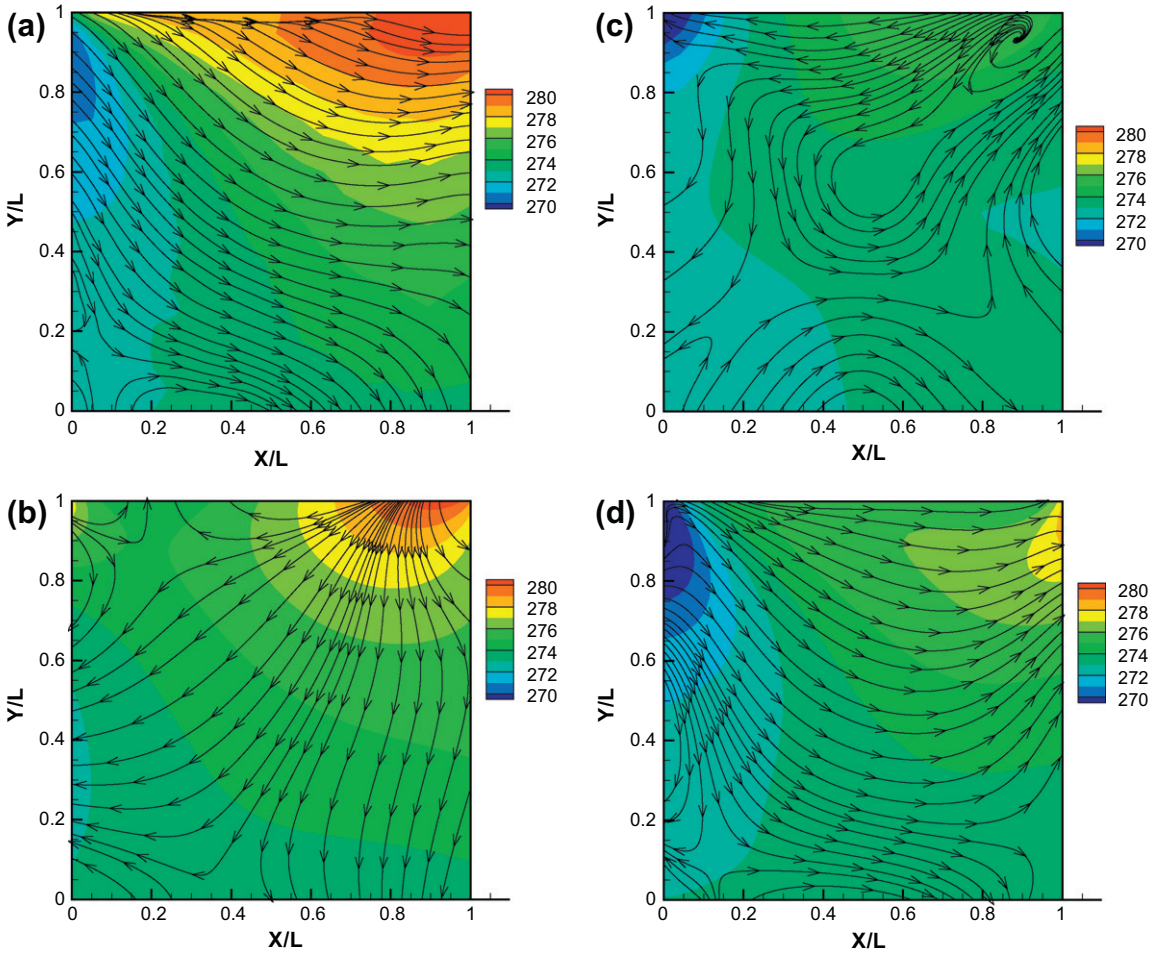

Fig. 4. Heat flux stream traces overlaid on the temperature $\overline{T}$ ($\overline{T} = (T_{xx}+T_{yy}+T_{zz})/3$) contours by (a) DSMC, (b) NSE, (c) TTKM and (d) MTKM for the case with all wall temperature 273 K, $U_w = 100$ m/s and $Kn = 0.2$.

length L of the cavity $Kn = l_0/L$, the Mach number Ma is defined by the upper lid velocity U_w and the initial gas state $Ma = U_w/\sqrt{\gamma RT_0}$, where γ is the specific heat ratio.

The numerical results from the MTKM, TTKM and NSE are compared with the DSMC solutions. The variable hard sphere (VHS) collision model has been used with a reference particle diameter of $d = 4.17 \times 10^{-10}$ m. The particle–wall interactions are assumed to be inelastic and follow the diffuse reflection model with the full thermal accommodation. In the present study, the uniform mesh is used and the cell size is set to be $\Delta x = \Delta y = 0.25 l_0$, which is small enough for all the numerical tests considered here. The time step is set to be $\Delta t = 0.125\Delta x(2R\overline{T}_{max})^{-1/2}$, where $\overline{T}_{max}$ is the maximum of the averaged temperature within the domain. 40 particles per cell have been employed for the initialization in the present work. The variation in Knudsen number Kn is achieved by changing the side length L of the cavity.

First we consider a test problem with large temperature gradients. The upper wall temperature is 273 K and all other wall temperature is 546 K, the upper lid velocity is $U_w = 15.39$ m/s with the corresponding Mach number $Ma = 0.05$, the Knudsen number is $Kn = 0.1$. Due to the large temperature gradients, this test case is not an easy one for many continuum-based approaches.

Fig. 1a shows the U-velocity along a vertical line crossing the cavity center by the previously mentioned four methods, where we can see that the numerical results by the NSE, TTKM and MTKM are similar and close to the DSMC solutions. Fig. 1b gives the V-velocity along a horizontal line crossing the center, where it is observed that compared with the DSMC data the overall performance of the MTKM is slightly better than the NSE and much better than the TTKM. Fig. 2 shows the contours of the temperature T_{xy} by the DSMC and the MTKM. The agreement between the DSMC and MTKM data is good. It should be pointed out here that the temperature T_{xy}, which is defined by

$$T_{xy} = \frac{1}{\rho R}\int (u-U)(v-V) f du dv dw, \tag{29}$$

can be zero or negative. From the definition we know that the relation between the temperature T_{xy} and the viscous stress τ_{xy} is $\tau_{xy} = -\rho R T_{xy}$, therefore, the non-positive values of T_{xy} in this figure can be easily understood.

The second test considers the case with all wall temperature 273 K, $U_w = 10$ m/s, and $Kn = 0.2$. Compared with the first example, the temperature gradients here are very small. In Fig. 3, a comparison of the DSMC, NSE, TTKM and MTKM is made for the contours of the averaged temperature $\overline{T}$, and the stream traces of the heat flux vector $\mathbf{q}$, which is defined as

$$q_i = \frac{1}{2}\int (u_i - U_i)(\mathbf{u}-\mathbf{U})^2 f du dv dw. \tag{30}$$

It can be seen from Fig. 3 that the contours of the averaged temperature $\overline{T}$ by the MTKM agree much better with those by the DSMC than the contours by the NSE and the TTKM. As shown and discussed in [29,30], the very interesting thing in Fig. 3 is that the heat flow direction predicted by the DSMC is from the cold to hot region under the non-equilibrium flow conditions. This indicates that a counter-gradient heat flux is possible due to various non-equilibrium effects like expansion cooling, viscous heat generation, compressibility and thermal creep, etc. Interested readers may refer to [30] for more discussions and explanations for this unusual phenomenon. In terms of the comparisons among the different models in describing this phenomenon, the NSE and the TTKM fail to capture this counter-gradient heat flux pattern, but the MTKM can capture this unusual phenomenon very well.

The third example is a relatively high speed case with all wall temperature $273K$, $U_w = 100$ m/s, and $Kn = 0.2$. The numerical results are shown in Fig. 4. Compared with the high reliable DSMC

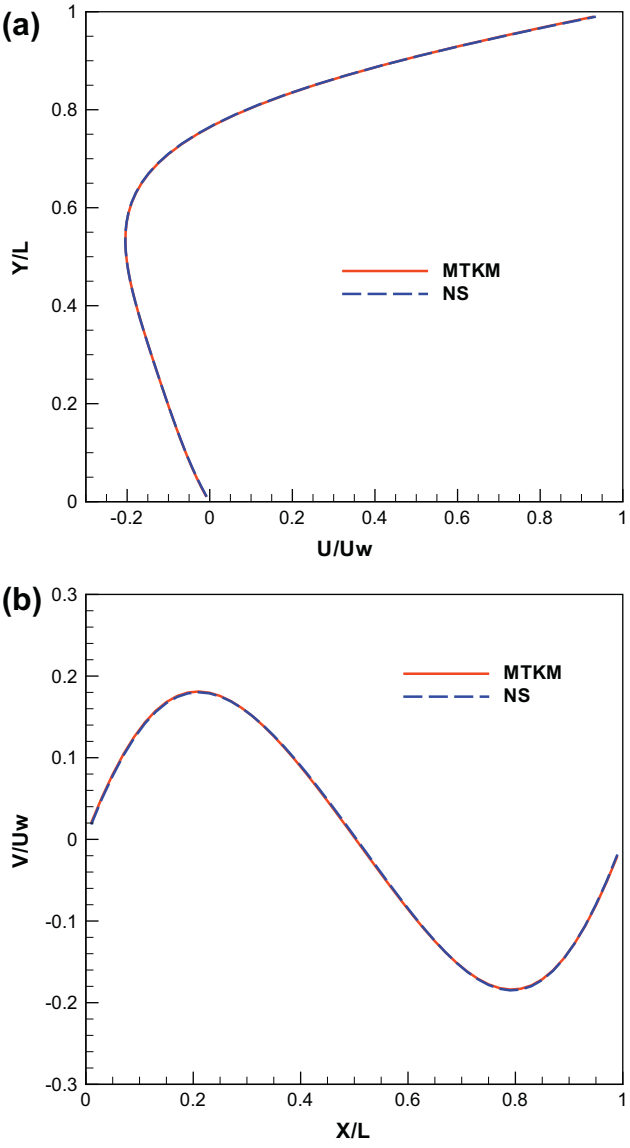

Fig. 5. Velocity profiles for the case with $Kn = 0.001$, $Re = 6.25$ ($Ma = 0.005$). (a): The U-velocity along a vertical line crossing the cavity center; (b): The V-velocity along a horizontal line crossing the cavity center.

method, the NSE cannot predict the cold region around the upper left corner, the TTKM performs better than the NSE but worse than the MTKM, which can capture the cold region well. Regarding to the hot region around the upper right corner, the results by the NSE and MTKM are closer to the DSMC data than those by the TTKM. Again, the counter-gradient heat flux phenomenon can be well captured by both the DSMC and the MTKM, but the NSE and the TTKM fail to capture it.

From the three numerical examples previously shown, we can see that the MTKM has the obvious advantages over the TTKM, in particular, the former can predict the counter-gradient heat transfer while the latter fails to do that. In fact the major differences between the two models are that for the MTKM the temperatures used in the intermediate Gaussian distribution g are assumed to be a symmetric second-order tensor, while for the TTKM they are only assumed to be three temperatures in the x-, y- and z-directions which are coordinate-dependent, in some sense this means artificially imposing the principal axes of the temperature tensor to be the computational coordinate axes everywhere.

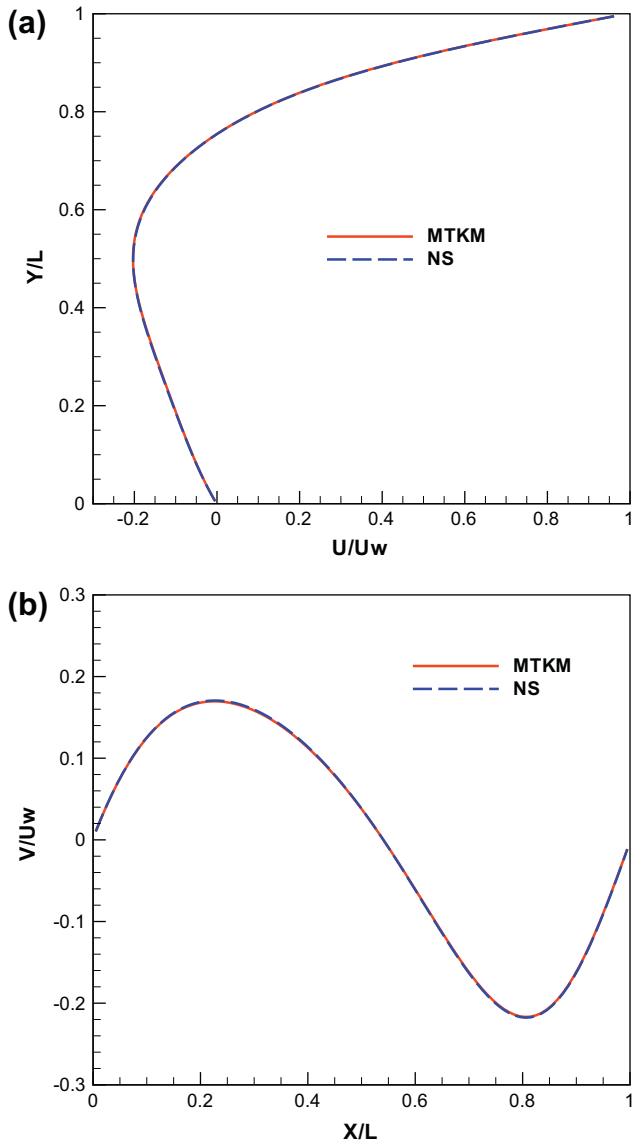

Fig. 6. Velocity profiles for the case with $Kn = 0.001$, $Re = 62.5$ ($Ma = 0.05$). (a): The U-velocity along a vertical line crossing the cavity center; (b): The V-velocity along a horizontal line crossing the cavity center.

Therefore, it is believed that physically the TTKM is less reasonable and accurate than the MTKM, which is also clearly demonstrated by the numerical tests presented.

Finally we want to investigate the performance of the MTKM at the continuum limit, i.e. $Kn \to 0$. Two examples with a small Knudsen number $Kn = 0.001$ are considered: $Ma = 0.005$ and $Ma = 0.05$, the corresponding Reynolds numbers ($Re = \rho_0 U_w L/\mu_0$) are $Re = 6.25$ and $Re = 62.5$, respectively. All wall temperature is 273 K in both cases. The numerical results are shown in Figs. 5 and 6, where the velocity profiles by the MTKM and the NSE cannot be distinguished by eyes. From the figures, we can see that the MTKM solutions can recover the NSE solutions at the continuum limit, which is consistent with the theoretical analysis in [1]. Therefore the MTKM can be faithfully used to study both continuum and near continuum gas flows.

4. Conclusions

A numerical algorithm for solving the MTKM is proposed, and the strategy used for the proposed method is similar to those in [2,31]. For the present gas-kinetic scheme, instead of using the macroscopic generalized gas dynamic equations directly to find the numerical fluxes across cell interfaces, based on the Chapman-Enskog expansion of the MTKM, the time-dependent gas distribution function f at the cell interface can be obtained. Then, it is used to calculate the numerical flux there by taking moments and time integration.

Many numerical tests have been used to validate the MTKM in the continuum and near continuum flow regimes. The micro-scale gas flow tests clearly demonstrate the advantages of the MTKM over the NSE and the early TTKM for modeling the non-equilibrium flows, especially in the cases with complicated flow structures. In the transition flow regime, the unusual counter-gradient heat flux phenomenon has been captured by the MTKM, but the NSE and the TTKM fail to do that. It is also numerically manifested that the NSE solutions can be recovered from the MTKM in the continuum limit ($Kn \to 0$). The multiple temperature kinetic model is useful in the study of micro-scale gas flows.

Acknowledgements

H. Liu would like to thank Mr. Songze Chen for providing the Mathematica program for the evaluation of the moments of Gaussian distribution and many helpful discussions. The authors also appreciate the unknown referees for their constructive comments and suggestions which greatly improve the manuscript. The current research was supported by Hong Kong Research Grant Council 621709, RPC10SC11, and National Natural Science Foundation of China (Project No. 10928205).

References

[1] Xu K, Guo Z. Multiple temperature gas dynamic equations for non-equilibrium flows. J Comput Math 2011;29(6):639–60.
[2] Xu K, Liu H, Jiang J. Multiple temperature kinetic model for continuum and near continuum flows. Phys Fluids 2007;19:016101.
[3] Fan J, Shen C. Statistical simulation of low-speed rarefied gas flows. J Comput Phys 2001;167:393–412.
[4] Sun Q, Boyd ID. A direct simulation method for subsonic, micro-scale gas flow. J Comput Phys 2002;179:400–25.
[5] Masters ND, Ye W. Octant flux splitting information preservation DSMC method for thermally driven flows. J Comput Phys 2007;226:2044–62.
[6] Zhang J, Fan J, Jiang J. Multiple temperature model for the information preservation method and its application to nonequilibrium gas flows. J Comput Phys 2011;230:7250–65.
[7] Baker L, Hadjiconstantinou N. Variance reduction for Monte Carlo solutions of the Boltzmann equation. Phys Fluids 2005;17:051703.
[8] Chun J, Koch D. A direct simulation Monte Carlo method for rarefied gas flows in the limit of small Mach number. Phys Fluids 2005;17:107107.
[9] Sun Q, Boyd ID, Candler GV. A hybrid continuum/particle approach for modeling rarefied gas flows. J Comput Phys 2004;194:256–77.
[10] Schwartzentruber TE, Scalabrin LC, Boyd ID. A modular particle-continuum numerical method for hypersonic non-equilibrium gas flows. J Comput Phys 2007;225:1159–74.
[11] Ohwada T. Structure of normal shock waves: direct numerical analysis of the Boltzmann equation for hard-sphere molecules. Phys Fluids A 1993;5:217–34.
[12] Yang JY, Huang JC. Rarefied flow computations using nonlinear model Boltzmann equations. J Comput Phys 1995;120:323–39.
[13] Li ZH, Zhang HX. Gas-kinetic numerical studies of three-dimensional complex flows on spacecraft re-entry. J Comput Phys 2009;228:1116–38.
[14] Xu K, Huang JC. A unified gas-kinetic scheme for continuum and rarefied gas flows. J Comput Phys 2010;229:7747–64.
[15] Aristov VV. Direct methods for solving the Boltzmann equation and study of nonequilibrium flows. Dordrecht, The Netherlands: Kluwer Academic Publishers.; 2001.
[16] Bobylev AV. The Chapman-Enskog and Grad methods for solving the Boltzmann equation. Sov Phys Dokl 1982;27:29–31.
[17] Zhong X, MacCormack RW, Chapman DR. Stabilization of the Burnett equations and application to hypersonic flows. AIAA J 1993;31:1036–43.
[18] Agarwal RK, Yun KY, Balakrishnan R. Beyond NavierCStokes: Burnett equations for flows in the continuum-transition regime. Phys Fluids 2001;13:3061.
[19] Ohwada T, Xu K. The kinetic scheme for the full-Burnett equations. J Comput Phys 2004;201:315–32.
[20] Grad H. On the kinetic theory of rarefied gases. Commun Pure Appl Math 1949;2:331–407.

[21] Struchtrup H, Torrilhon M. Regularization of Grad's 13 moment equations: derivation and linear analysis. Phys Fluids 2003;15:2668–80.
[22] Gu XJ, Emerson DR. A high-order moments approach for capturing non-equilibrium phenomena in the transition regime. J Fluid Mech 2009;636:177–216.
[23] Levermore CD. Moment closure hierarchies for kinetic theories. J Stat Phys 1996;83:1021–65.
[24] Xu K, Liu H. A multiple temperature kinetic model and its application to near continuum flows. Commun Comput Phys 2008;4(5):1069–85.
[25] Xu K, Tang L. Nonequilibrium Bhatnagar-Gross-Krook model for nitrogen shock structure. Phys Fluids 2004;16(10):3824–7.
[26] Cai C, Liu DD, Xu K. One-dimensional multiple-temperature gas-kinetic Bhatnagar–Gross–Krook scheme for shock wave computation. AIAA J 2008;46(5):1054–62.
[27] Naris S, Valougeorgis D. The driven cavity flow over the whole range of the Knudsen number. Phys Fluids 2005;17:097106.
[28] Sun Q, Li F, Fan J, Cai C. Development of an efficient particle approach for micro-scale gas flow simulations. In: Proceedings of MNHMT09, MNHMT2009-18291; 2009.
[29] Gu XJ, John B, Tang GH, Emerson DR. Heat and mass transfer of a rarefied gas in a driven micro-cavity. In: Proceedings of MNHMT09, MNHMT2009-18236; 2009.
[30] John B, Gu XJ, Emerson DR. Investigation of heat and mass transfer in a lid-driven cavity under nonequilibrium flow conditions. Numer Heat Transfer, Part B: Fundam 2010;58(5):287–303.
[31] Xu K. A gas-kinetic BGK scheme for the Navier–Stokes equations and its connection with artificial dissipation and Godunov method. J Comput Phys 2001;171:289–335.
[32] Xu K, Li Z. Microchannel flow in the slip regime: gas-kinetic BGK-Burnett solutions. J Fluid Mech 2004;513:87–110.
[33] Li QB, Fu S, Xu K. Application of gas-kinetic scheme with kinetic boundary conditions in hypersonic flow. AIAA J 2005;43(10):2170–6.